buildings

MDPI

Article

Shear Performance of Assembled Bamboo–Concrete Composite Structures Featuring Perforated Steel Plate Connectors

Lingling Chen [1], Zhiyuan Wang [2,*] and Huihui Liu [2]

[1] School of Civil and Hydraulic Engineering, Bengbu University, Bengbu 233030, China; cll@bbc.edu.cn
[2] School of Management Science and Engineering, Anhui University of Finance and Economics, Bengbu 233030, China; 120081721@aufe.edu.cn
* Correspondence: 120150012@aufe.edu.cn

Abstract: To reduce the cast in place work of concrete and realize the industrial production of a bamboo–concrete composite (BCC), innovative connection systems composed of an assembled bamboo–lightweight concrete composite (ABLCC) structure featuring perforated steel plate connectors are presented for use in engineering structures. This study examined the shear performance of connection systems composed of an assembled BCC structure featuring perforated steel plate connectors based on the design and fabrication of three groups of shear connectors with nine different parameters using bamboo scrimber, lightweight concrete, perforated steel plates, and grout. Push-out tests were conducted on these shear connectors. A linear variable differential transformer (LVDT) and digital image correlation (DIC) were utilized for measurements. The test parameters comprised fabrication techniques (assembled and cast-in-place/CIP) and connector size (steel plate thickness). This study investigated mechanical performance indicators, including the failure mode, load–slip relationship, shear stiffness, and shear capacity of the shear connectors. The experimental results showed that the shear connector failure modes involved concrete spalling near the connectors and deformation of the perforated steel plates. The load–slip curves generally included three stages: high slope linear increase, low slope nonlinear increase, and rapid decrease. The shear capacity and stiffness of the assembled shear connectors were 0.84 times and 2.46 times those of the CIP connectors, respectively. The stiffness of the 4 mm steel plate connectors increased by 42% compared to the 2 mm steel plate connectors. Analysis showed that the shear capacity of the BBC primarily consisted of four aspects: the end bearing force of the steel plate, contact friction, and forces due to the influence of tenon columns and the reinforcing impact of through-rebars. This study proposes a simple and suitable formula for obtaining the shear capacity of perforated steel plate connectors in the BCC structure, with the analytical values being in good agreement with the test results.

Keywords: bamboo–concrete composite structure; shear performance; perforated steel plate connector; analytical investigation; digital image correlation

check for updates

Academic Editor: Salvatore Verre

Received: 23 March 2025
Revised: 14 April 2025
Accepted: 17 April 2025
Published: 21 April 2025

Citation: Chen, L.; Wang, Z.; Liu, H. Shear Performance of Assembled Bamboo–Concrete Composite Structures Featuring Perforated Steel Plate Connectors. *Buildings* **2025**, *15*, 1376. https://doi.org/10.3390/buildings15081376

Copyright: © 2025 by the authors. Licensee MDPI, Basel, Switzerland. This article is an open access article distributed under the terms and conditions of the Creative Commons Attribution (CC BY) license (https://creativecommons.org/licenses/by/4.0/).

1. Introduction

The steady decline in global forest areas since the 1990s highlights the need for a sustainable alternative to wood in construction. Bamboo, known for its high tensile and compressive strength, has emerged as a promising solution [1]. Researchers have developed different types of reinforced bamboo flexural components, including bamboo–concrete composite (BCC) beams, as novel composite component [2]. In BCC beams, concrete, known for its strong compressive strength, is placed in the upper compression zone of

the composite beam, and bamboo, known for its excellent tensile properties, is placed in the lower tension zone. These two materials are connected by shear connectors, allowing them to function as a united system. Compared to pure bamboo beams, BCC beams offer superior flexural mechanical properties such as flexural capacity and stiffness. For example, Wang et al. [3] subjected 10 BCC beams to four-point bending tests and demonstrated that the ultimate load of the BCC beams was 1.2–1.5-fold higher than that of bamboo beams, while the sectional stiffness of the BCC beams was elevated by 2.9–4.2 folds. Moreover, Shan et al. [4] performed experiments using nine full-scale 8 m BCC beams with varying connector types under four-point bending failure. The results showed that BCC beams with different connectors all showed excellent flexural performance under short-term loads, and BCC beams with notched connectors demonstrated exceptional flexural capacity. Li et al. [5] conducted static bending tests on five 5 m BCC beam specimens and found that BCC beams with UHPC–steel composite connections exhibited superior bending performance.

When BCC beams undergo flexural deformation, axial shear is generated at the interface of the bamboo beam and concrete flange. This longitudinal shear is transferred by shear connectors [6], thereby limiting the relative slip between the bamboo beam and concrete flange. Consequently, the shear performance of the connectors directly influences the flexural performance of BCC beams, which necessitates the study of the shear performance of the shear connectors. Shan et al. [7] developed a novel reactive powder concrete (RPC)–steel shear connector and conducted push-out tests, demonstrating that the RPC–steel shear connector exhibited superior shear performance. In addition, a parametric model was proposed to predict the shear stiffness and shear capacity of the composite connector. Xiao et al. [8] utilized six types of shear connectors for BCC beams in push-out tests and demonstrated that, different from connectors for timber–concrete composite components, the most suitable connectors for BCC beams included notched, steel mesh, screw, and prestressed dowel + notched connectors. Wang et al. [9] conducted push-out tests utilizing 18 bamboo–concrete shear connectors and 18 timber–concrete shear connectors and found that the failure modes of bamboo–concrete specimens were comparable to the failure modes of timber–concrete specimens; moreover, the shear stiffness and shear capacity of the bamboo–concrete connectors were elevated in comparison to those of timber–concrete connectors, where the shear capacity rose with the diameter of the connecting dowels and the concrete strength. Chen et al. [10] subjected bamboo–concrete shear connectors with perforated steel plates to push-out tests and found that as the strength of the concrete increased, enhancements were observed in the stiffness and load capacity of the connector, and when the diameter of the perforations in the steel plate was greater, the results revealed a lower connection stiffness and larger slip corresponding to the ultimate load.

In summary, previous investigations regarding the mechanical performance of BCC structures have mainly examined bamboo–cast-in-place (CIP) concrete composite components. However, BCC structures possess drawbacks, including their heavy weight, complex processing technology, and slow processing speed. The present study utilized lightweight concrete rather than normal concrete to decrease the weight of the BCC structures. Prefabricated concrete was employed rather than CIP concrete to eliminate field tasks such as formwork installation, rebar tying, and concrete casting and accelerate the speed of construction. Fast-curing, early-strength grout was used with connectors to achieve a grout–anchor connection for the composite beam assembly. While the grout was more expensive than regular concrete, only a small amount was needed. Therefore, using high-strength grout had little impact on the overall budget; however, the connection strength was enhanced, and the local stress concentration at the connections improved. During the assembly process, semicircular U-shaped notches on the upper portion of the new

perforated steel plates enabled the easy passage of the through-rebars embedded in the concrete, thus facilitating rapid assembly.

In this study, we carried out the structural design of the connection system for assembled BCC beams and investigated its shear performance through experimental testing and analysis. The preliminary experimental data and mechanical indicators have been promptly reported in the literature [11]. This paper provides a detailed description of the shear connector fabrication process in addition to a corresponding analysis of the failure process based on the test data. The DIC data collected in subsequent analyses were examined, and the failure modes of the specimens were utilized to conduct a detailed exploration of the force mechanism of the connection system. The present study employed relevant analytical research methods to investigate the shear capacity of the connectors, with the goal of deriving a shear capacity calculation method.

2. Experimental Program

2.1. Material Properties

2.1.1. Bamboo

The bamboo scrimber used in this test was manufactured through hot-pressing technology, with the production process comprising round bamboo slicing, rolling into strand bundles, drying, resin impregnation, mat formation after secondary drying, and hot-pressing molding. Based on the ASTM D143-09 standard [12], 10 bamboo scrimber compressive specimens measuring 30 × 20 × 20 mm were prepared for the experiments, with the length in the grain direction being 30 mm for all specimens. A further 10 tensile specimens measuring 20 × 15 × 370 mm were prepared for the tests, as illustrated in Figure 1. The mechanical properties of the bamboo scrimber were as follows: a compressive strength along the grain of 104.07 MPa, a compressive elastic modulus of 13.43 GPa, a tensile strength along the grain of 149.62 MPa, and a tensile elastic modulus of 16.81 GPa. Table 1 displays the test results.



(**a**) compressive test specimen



(**b**) tensile test specimen

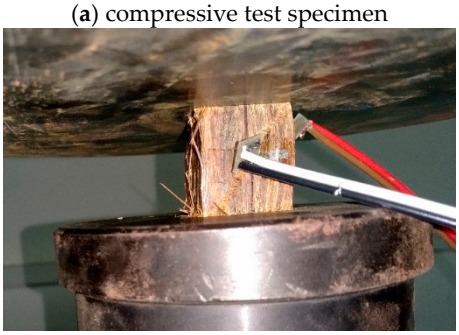

(**c**) compressive test

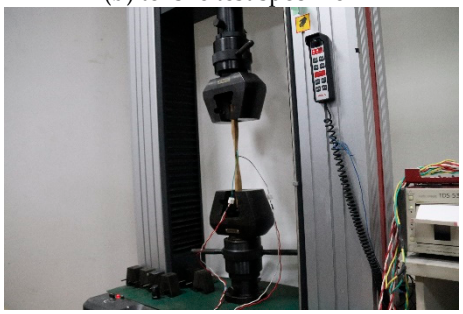

(**d**) tensile test

Figure 1. *Cont.*



(**e**) failure mode of the compressive specimens



(**f**) failure mode of the tensile specimen

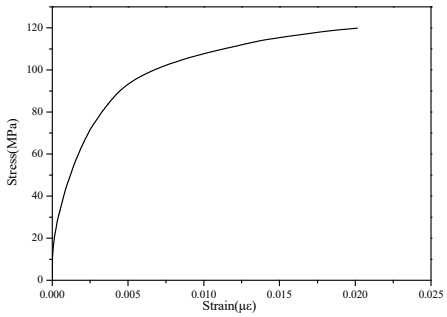

(**g**) stress-strain curve of a compressive specimen

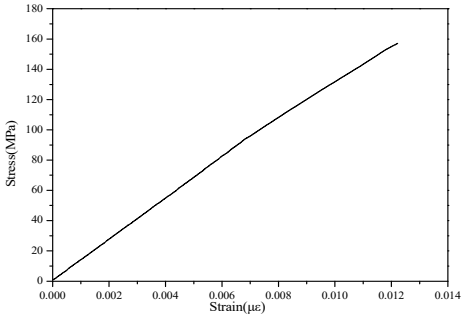

(**h**) stress-strain curve of a tensile specimen

Figure 1. Mechanical performance test of bamboo scrimber tensile specimens.

Table 1. Materials properties of bamboo.

Property	Number of Specimens	Average Value	Standard Deviation	Coefficient of Variation (%)
Tensile strength (MPa)	10	149.62	15.91	10.63
Tensile strain	10	0.009	0.002	22.17
Tensile modulus of elasticity (GPa)	10	16.81	2.91	17.33
Compressive strength (MPa)	10	104.07	12.24	11.77
Compressive strain	10	0.031	0.012	40.43
Compressive modulus of elasticity (GPa)	10	13.43	5.77	42.98

2.1.2. Concrete

With reference to the GB/T 50081-2019 standard [13], three lightweight concrete cylinder specimens (φ150 × 300 mm) and three cube specimens (150 × 150 × 150 mm) were prepared for the tests at a concrete mix ratio of 1:0.29:0.89:1.34:0.23 (cement:water:sand:haydite:water reducer). Table 2 displays the results of the testing.

Table 2. Materials properties of lightweight concrete.

Specimen Type	Specimen	Mass (kg)	Density (kg/m^3)	Ultimate Compressive Load (kN)	Compressive Strength (MPa)
Cube specimen	CU-1	6.39	1893.33	944.30	41.97
	CU-2	6.24	1848.89	965.00	42.89
	CU-3	6.28	1860.74	922.50	41.00
	Mean	6.30	1867.65	943.93	41.95
	SD	0.06	18.79	17.35	0.77
	COV	1.01%	1.01%	1.84%	1.84%

Table 2. *Cont.*

Specimen Type	Specimen	Mass (kg)	Density (kg/m^3)	Ultimate Compressive Load (kN)	Compressive Strength (MPa)
Cylinder specimen	CY-1	9.59	1809.86	635.20	35.96
	CY-2	9.82	1853.27	626.80	35.49
	CY-3	9.61	1813.64	617.70	34.97
	Mean	9.67	1825.59	626.57	35.47
	SD	0.10	19.63	7.15	0.40
	COV	1.08%	1.08%	1.14%	1.14%

2.1.3. Steel Plate

To determine the mechanical properties of the steel plates, this study referred to Metallic Materials—Tensile Testing—Part 1: Method of Test at Room Temperature (GB/T 228.1-2010) [14]. For tensile testing, five 2-milimeter-thick and five 4-milimeter-thick steel plate specimens were prepared (Figure 2). The test measurements revealed that the 2-milimeter-thick steel plates exhibited a yield strength of 324.4 MPa, an elastic modulus of 199.3 GPa, an ultimate tensile strength of 481.29 MPa, and an elongation of 21.7%, while the 4-milimeter-thick steel plates showed a yield strength of 263.4 MPa, an elastic modulus of 201.7 GPa, an ultimate tensile strength of 378.45 MPa, and an elongation of 21.2%.

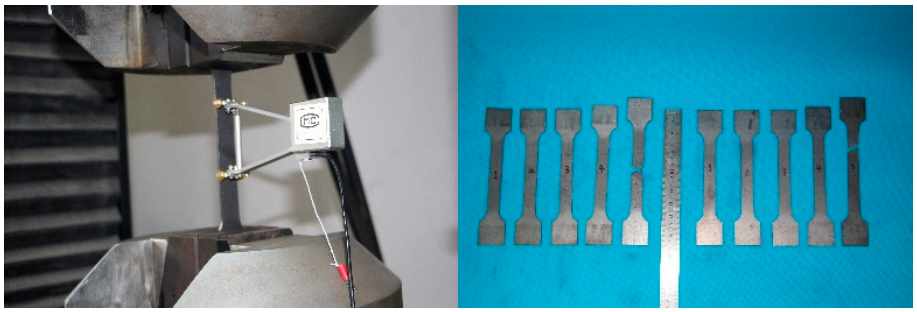

(**a**) tension device (**b**) steel plated after tensile testing

Figure 2. Tension test of steel plates.

2.1.4. Grout

This study determined the mechanical properties of the grout following the Technical Code for the Application of Cementitious Grout (GB/T 50448-2015) [15]. Prior to testing, three cementitious grout cube specimens measuring 40 × 40 × 160 mm were prepared (Figure 3). First, a flexural test was conducted, followed by compressive tests on the two ends of each broken specimen from the flexural test. The grout used in the tests consisted of high-fluidity, high-strength, nonshrink cementitious grout (model H-40, Nanjing Hand Special Building Materials Co., Ltd., Nanjing, China). Table 3 displays the test results.



(**a**) flexural test (**b**) flexural failure (**c**) compressive failure

Figure 3. Grouting materials test.

Table 3. Material properties of the grout.

Specimen	Flexural Capacity (kN)	Flexural Strength (MPa)	Compressive Capacity (kN)	Compressive Strength (MPa)
G1	3.42	8.02	93.48 89.50	58.43 55.94
G2	3.55	8.32	85.50 99.38	53.44 62.11
G3	3.67	8.60	87.17 82.22	54.48 51.39
Mean	3.55	8.31	89.54	55.96
SD	0.10	0.24	5.60	3.50
COV	2.85%	2.88%	6.25%	6.25%

2.1.5. Adhesive

An epoxy resin adhesive (model L-500, Sanyu Co., Ltd., Osaka, Japan) was employed during testing. This adhesive was mainly utilized to connect the perforated steel plate to the bamboo to ensure stress transfer between the two materials and eliminate sliding friction between them. According to the manufacturer's information, the relevant physical and mechanical properties consisted of a tensile strength of 30 MPa, a flexural strength of 40 MPa, a tensile shear strength of 10 MPa, a compressive strength of 70 MPa, and a compressive elastic modulus of 1.0×10^3 MPa.

2.2. Design of the Shear Connections

This study referred to relevant publications to design the push-out test to examine the mechanical behavior of the bamboo–lightweight concrete connection specimens [6–10] as bamboo–concrete shear connectors. Three specimens were fabricated for each type of connector, with the specimen parameters listed in Table 4. To achieve superior connection performance, including convenient assembly and increased shear strength, this study designed a special type of perforated steel plate to serve as the connector, as described below.

Table 4. Push-out test shear connection parameters [11].

Specimen Group	Specimen ID	Thickness of the Perforated Steel Plate (mm)	Fabrication Method	Number of Specimens
BPC02A	BPC02A-1/2/3	2	Assembly	3
BPC04A	BPC04A-1/2/3	4	Assembly	3
BPC04P	BPC04P-1/2/3	4	CIP	3

Note: B: Bamboo. P: Plate. C: Concrete. A: Assembling. P: Pouring.

The shear connection specimen comprised a single bamboo block measuring 70 × 140 × 350 mm (width × height × length) and two concrete blocks, each measuring 70 × 140 × 350 mm (width × height × length) (Figure 4). The central bamboo block was connected to the two side concrete blocks using a perforated steel plate connector to form the overall shear connection specimen.

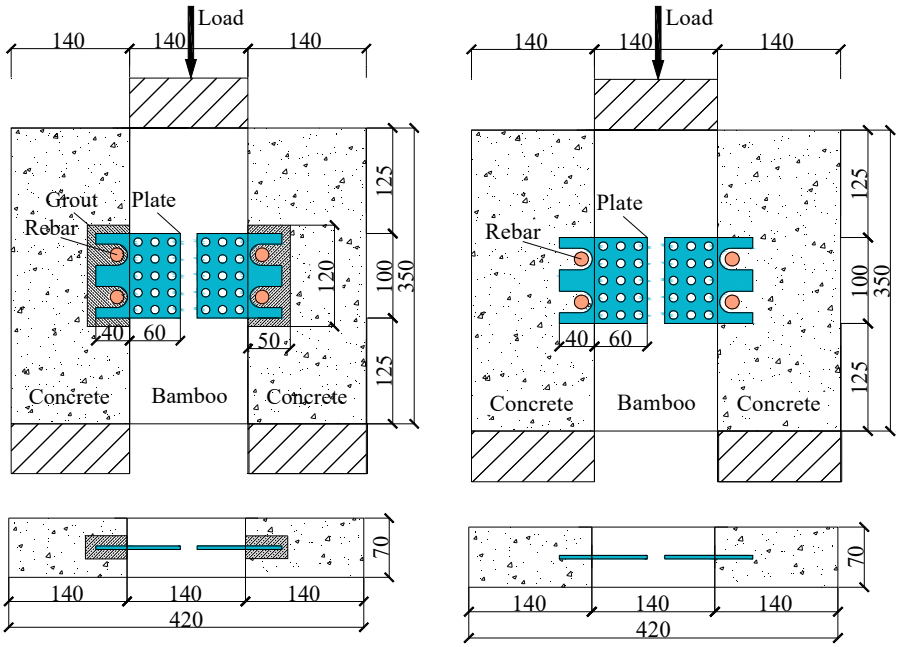

(**a**) assembled specimen (**b**) bamboo–cast-in-place (CIP) specimen

Figure 4. Details regarding the push-out tests of bamboo–lightweight concrete shear specimens (mm).

In the prefabricated concrete blocks, 12-milimeter-diameter through-rebars were installed, and φ6 threaded rebars were arranged as constructional reinforcement. The notch in the concrete block, i.e., the grout block, had dimensions of 120 × 35 × 50 mm (length × width × depth). The connector employed a novel perforated steel plate with dimensions of 100 × 100 × 2 mm (or 4 mm) and an embedment depth of 60 mm into the bamboo and 40 mm into the concrete. The top of the perforated steel plate included a row of two columns of 25-milimeter-wide semicircular U-shaped notches, which enabled the through-rebars to pass through and anchor in the steel plate notches in the assembly process to achieve a connection effect comparable to that of the PBL connectors [16]. Three rows of five columns of small 10-milimeter-diameter perforations at the bottom of the perforated steel plate allowed for the generation of structural adhesive shear tenons in the bamboo beam notches following adhesive injection, thereby increasing the strength of the connection between the steel plate and the bamboo.

The specimen naming convention was as follows: B indicated bamboo, P represented plate, C referred to concrete, A denoted assembly, and P represented pouring. For example, the BPC04A specimen consisted of an assembled bamboo–CIP concrete specimen featuring a 4-milimeter-thick perforated steel plate. In addition, -1/-2/-3 added to the terms used for each specimen indicate the three specimens with the same parameters in each group.

Existing studies mostly focused on CIP concrete components in BCC beams; however, few studies have examined the mechanical performance of BCC beams assembled with prefabricated concrete components. Consequently, there is uncertainty regarding whether the assembly method adversely impacts the mechanical performance of the connectors. To address this uncertainty, the test parameters utilized in the present study also included the fabrication methods (assembled or CIP) to assess the feasibility of the assembly method.

2.3. Construction of the Shear Connections

The process employed to fabricate the assembled specimen with the perforated steel plate is depicted in Figure 5, with the overall assembly process displayed in Figure 5a. As shown in Figure 5b, the bamboo block was slit, the adhesive was injected, and the perforated steel plate was pre-embedded, featuring a slit depth of 60 mm and a slit width

of 0.5 mm greater than the perforated steel plate thickness. As shown in Figure 5c, the prefabricated concrete block had a reserved slot measuring 35 mm (width) × 140 mm (height) × 50 mm (depth), and the position of the embedded through-rebars corresponded to the location of the perforations in the steel plate. The cementitious grout was then injected into the concrete slot (Figure 5d). Figure 5e illustrates the assembly of the bamboo block and concrete block, with the exposed portion of the perforated steel plate pre-embedded in the bamboo block inserted into the grout during assembly.

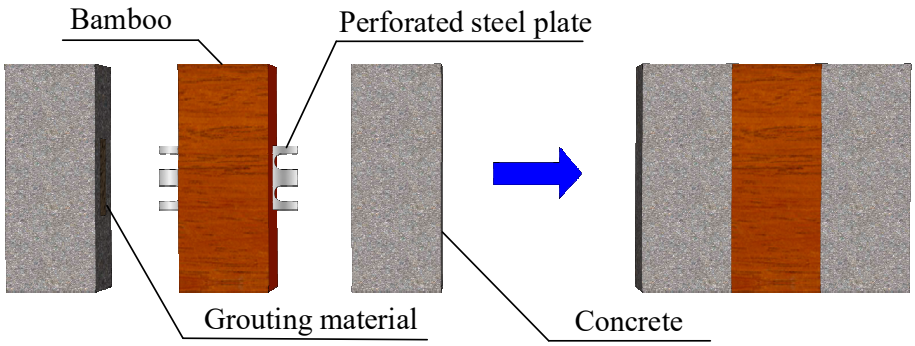

(**a**) assembly process schematic

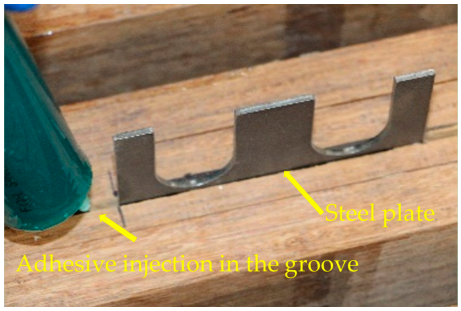

(**b**) embedding of a perforated steel plate

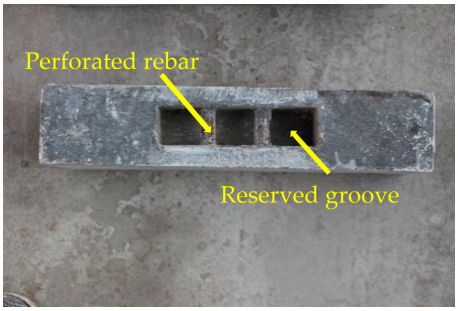

(**c**) prefabricated lightweight concrete block exhibiting a reserved slot

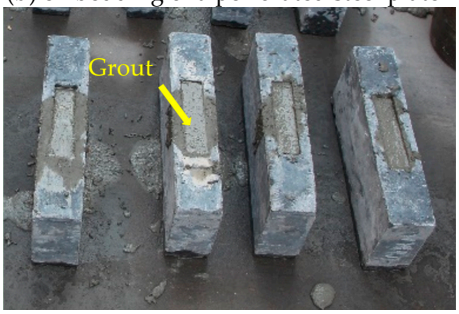

(**d**) grouting



(**e**) assembly

Figure 5. Fabrication of an assembled bamboo–lightweight concrete shear connection featuring perforated steel plate connectors.

The process employed to fabricate the CIP specimen with the perforated steel plate is depicted in Figure 6. The bamboo was first perforated or slotted, after which the perforated steel plate was embedded. The bamboo block with connectors was placed into the formwork before the assembled rebar cage was positioned. Finally, concrete was cast in place on either side of the bamboo block.



(**a**) Putting up the formwork (**b**) Pouring the concrete

Figure 6. Fabrication of the bamboo–cast-in-place (CIP) bamboo–lightweight concrete composite shear connections.

2.4. Shear Connection Test Setup

A 3000 kN high-stiffness rock testing machine was employed as a loading apparatus during this experiment (Figure 7). During the procedure, each specimen was preloaded multiple times with 5 and 10 kN to avoid the influence of gaps in the specimen. Formal loading was performed using a loading rate of 0.2 mm/min. As the load on the specimen exceeded the ultimate load and began to decrease continuously, the loading rate gradually rose to 0.5 mm/min until the conclusion of testing.

The relative slip between the bamboo scrimber and concrete was determined using two measurement techniques to collect real-time data on the interfacial slip using a linear variable displacement transducer (LVDT) and digital image correlation (DIC). When determining the relative slip of the shear connectors, the LVDT technique only yielded slip values at limited locations, which made capturing the distribution of relative slip challenging. However, the DIC technique enabled the collection of full-field displacement under the loading process, making it possible to calculate the relative slip values at all positions on either side of the bamboo–concrete interface. This allowed for the analysis of the distribution pattern of relative slip along the interface height, facilitating a more in-depth analysis of the slip distribution and enabling a comprehensive assessment of the load–slip relationship. Both LVDT and DIC were used in this study, and their data were cross-verified to ensure accuracy while minimizing the issues of local data loss from LVDT or DIC caused by localized specimen damage.

Regarding the LVDT setup, LVDT measurements were performed on the front of each specimen. Four LVDTs were symmetrically placed on the concrete blocks close to the interface, aligning the displacement gauge rods with the bamboo block angle steel baffles on the same plane. Data from the displacement transducers were collected using a TDS-530 data acquisition instrument, with measurements obtained at 3 s intervals.

The DIC setup employed in this study was as follows. The back side of each specimen was utilized to perform DIC measurements. Before DIC measurements, the surface of the specimen was polished and cleaned; after this, white and black paint were applied to the surface to design a pattern of uniformly distributed black speckles, which was necessary for the DIC camera to recognize the specimen. The surface was first coated with white matte paint as a primer, and after curing, black paint was sprayed. Prior to testing, a flat calibration plate was set on the surface of the specimen for the calibration of the DIC system. After the calibration images were analyzed and approved by the software, the test was initiated, and images of the specimens were collected. During the test, two image capture devices, set at specific angles, continuously collected images of specimen deformation throughout the experiment. The images were captured at a frequency of once every 3 s. Then, full-field relative slip at the interface was calculated. The image acquisition devices and VIC-3D image processing software were obtained from Correlated Solutions,

Columbia, SC, USA. The specifications of the camera included a focal length of 25 mm, a resolution of 12 million pixels, and a displacement measurement resolution of 1%. When loading officially started, both the LVDTs and DIC analysis began collecting experimental data simultaneously.

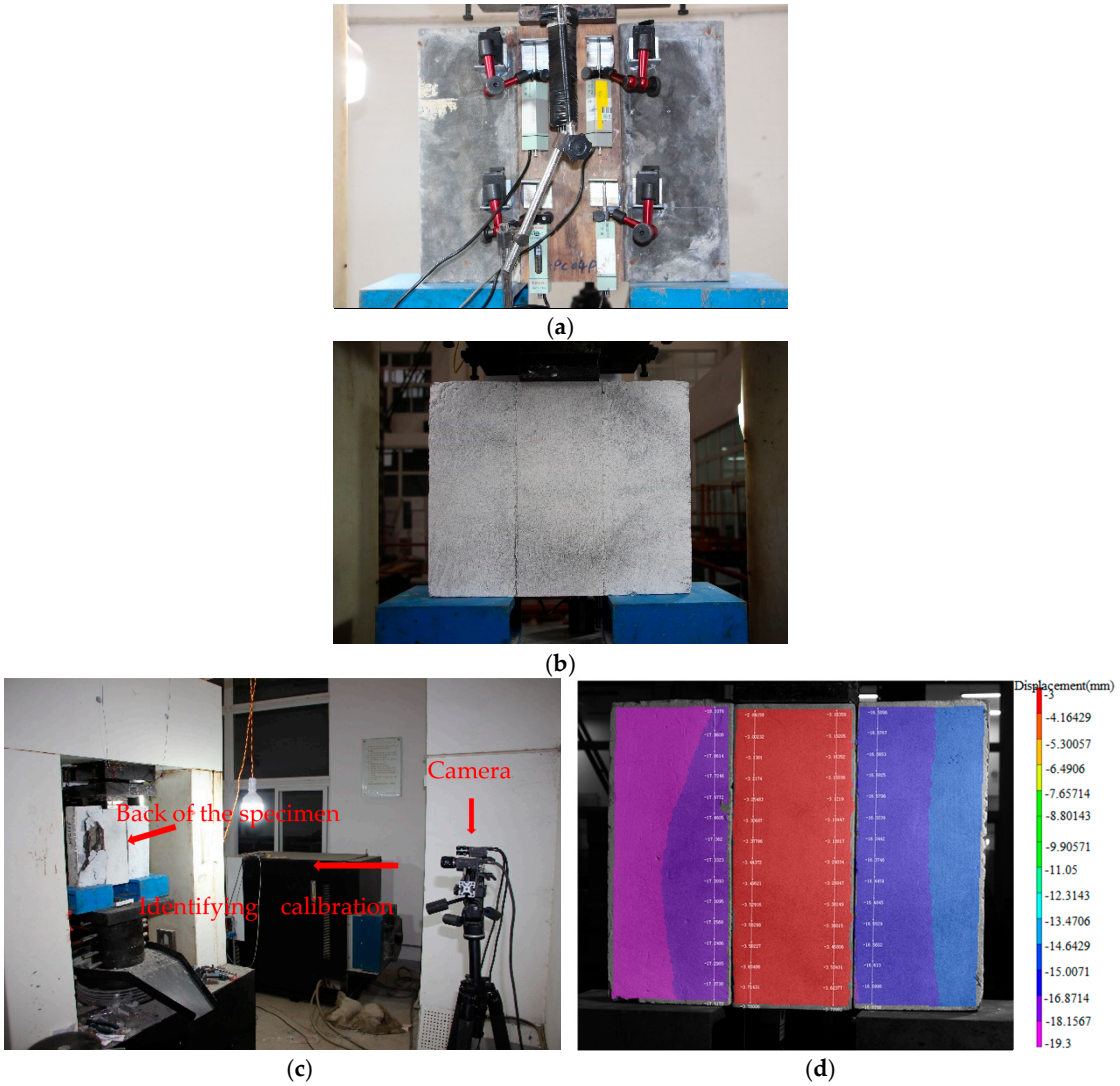

Figure 7. Detailed push-out test setup and measurement methods. (**a**) Linear variable differential transformer (LVDT) device on the front of the shear connector [11]. (**b**) Digital image correlation (DIC) speckle pattern on the back of the shear connector. (**c**) DIC measurements. (**d**) Displacement contours of the specimen surface determined using DIC.

3. Results and Discussion

3.1. Observations and Failure Modes

During the early loading stage, the appearance of the specimen exhibited no evident changes (Figures 8 and 9). As the load rose to approach the ultimate load P_{max}, the surface of the specimen did not appear damaged. However, as the load reduced to around 0.8 P_{max}, the concrete began to exhibit cracks. As the test progressed, the cracks developed slowly. The damage was primarily related to the deformation of the perforated steel plate, in addition to small areas featuring concrete spalling, which led to extensive slippage between the bamboo and concrete that ultimately resulted in connection failure. The bamboo material did not exhibit significant damage, with an insignificant difference in the failure modes between the CIP and assembled specimens.

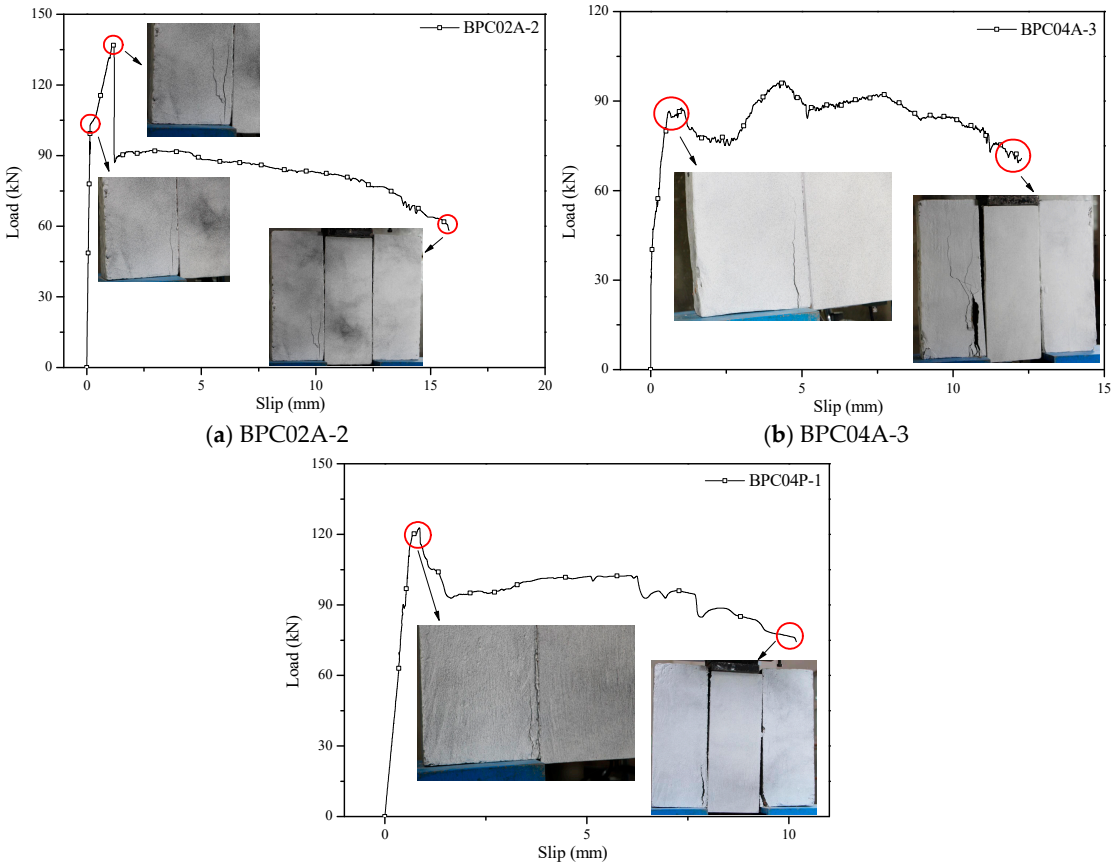

(**a**) BPC02A-2 (**b**) BPC04A-3

(**c**) BPC04P-1

Figure 8. Failure modes of the shear specimens featuring perforated steel plate connectors.



(**a**) local concrete spalling (**b**) perforated steel plate deformation

Figure 9. Failure mode of the shear specimens featuring perforated steel plate connectors.

3.2. Load–Slip Curves and Slip Distribution

Figure 10 displays multiple representative load–slip curves obtained using the LVDTs and DIC at symmetrical positions on the front and back of the shear connectors. The load–slip curves determined using the LVDTs and those obtained utilizing DIC were strongly correlated. The LVDT measurements were obtained from the front surface of the specimen, while the DIC data captured the deformation of the rear surface. Although both measurement systems monitored the same planar locations on opposite sides, certain discrepancies existed between the front and rear surfaces in terms of concrete cracking patterns and failure mechanisms.

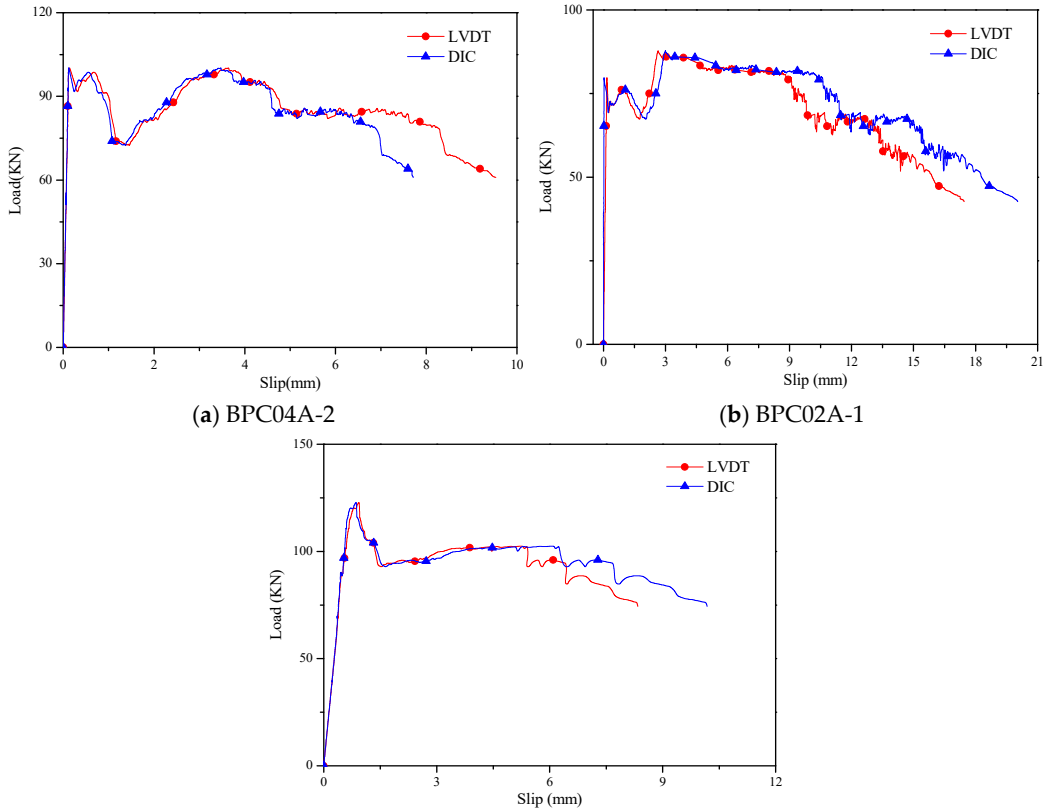

Figure 10. Load–slip curves of the shear connections obtained using two methods.

Moreover, the DIC technique, through image processing, could be employed to determine the full-field displacement contours of the surface of the specimen. Using DIC, the relative slip values were determined at 13 different heights along the interface to examine the slip distribution under different load levels in this study. Figure 11 depicts the curves indicating the slip variations along the interface height. The results revealed consistency between the slip values on both the left and right sides of the specimen, demonstrating that no eccentric loading occurred during the loading process before the ultimate load was reached, which led to uniform loading on the connectors of both sides. During the early loading stage, the line connecting the slip values of 13 measurement points at different heights exhibited an approximately linear trend, showing no sharp changes in slip values, which indicated that force transfer via the connector was stable. Under an increasing load with the same increment, the spacing between these connecting lines was enhanced, reflecting a steady decrease in the shear stiffness of the specimen, which was associated with the local failure of the concrete in addition to the yielding deformation of the connector. Among specimens featuring a perforated steel plate, the connecting lines of the specimens that included 4-milimeter-thick steel plates (BPC04P and BPC04A) did not exhibit abrupt changes, while abrupt changes were observed in the connecting lines of the specimen with 2-milimeter-thick steel plates (BPC02A). Considering the experimental observations, it was preliminarily concluded that the reduced thickness of the 2-milimeter-thick steel plate induced the local failure of the structural adhesive at the connection points due to the insufficient shear capacity caused by the smaller volume of the adhesive tenon within the perforations in the thinner steel plate.

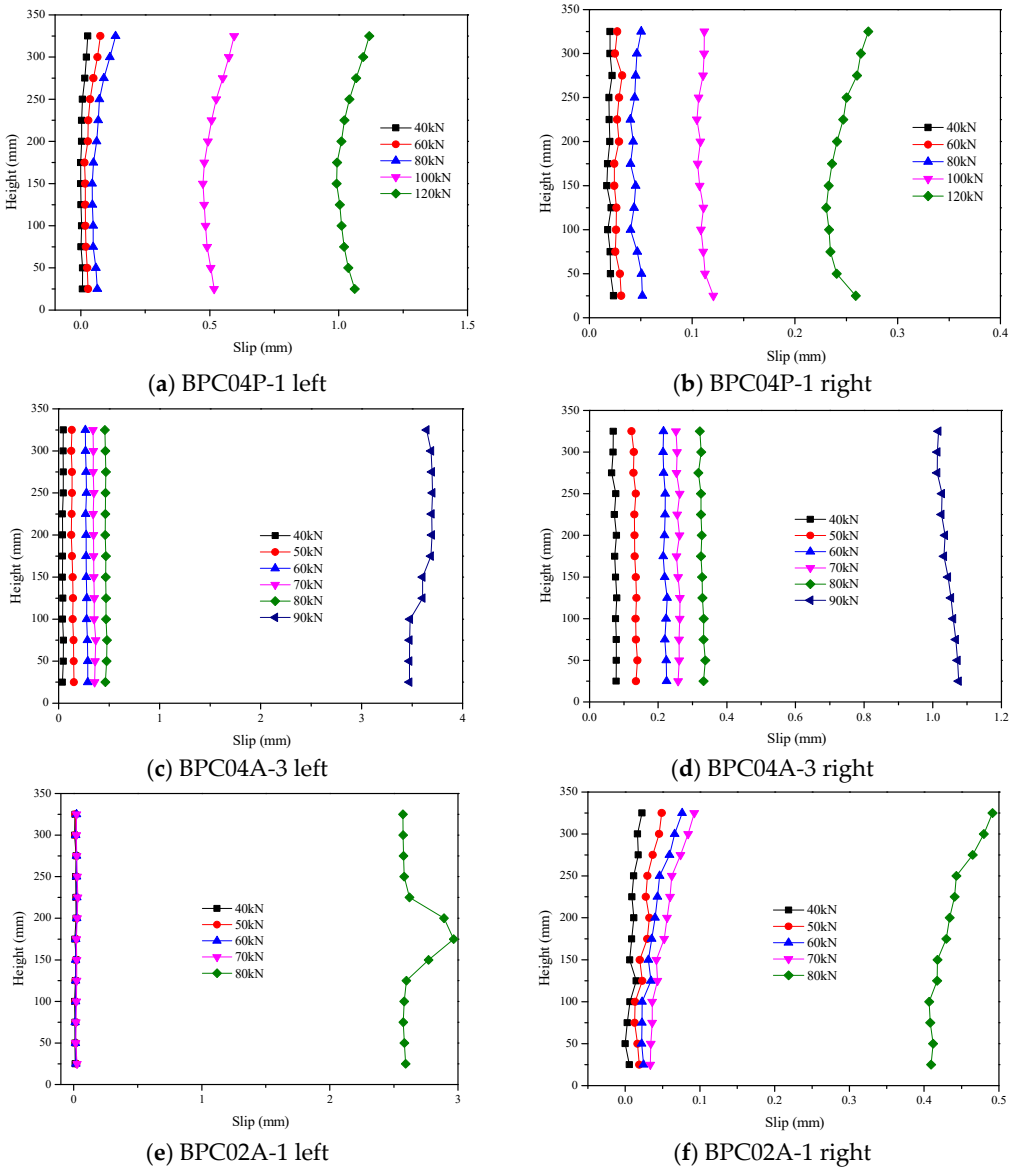

(**a**) BPC04P-1 left (**b**) BPC04P-1 right

(**c**) BPC04A-3 left (**d**) BPC04A-3 right

(**e**) BPC02A-1 left (**f**) BPC02A-1 right

Figure 11. Curves of the slip of shear specimens along the interface height.

3.3. Flexural Stiffness and Capacity

Table 5 provides the shear stiffness and capacity of the bamboo–concrete connectors. Because each shear specimen included two connectors, the shear stiffness of a single connector was calculated as half of the total shear stiffness. The initial stiffness of each specimen was calculated as 0.4 times the maximum load divided by the corresponding displacement to examine the initial stiffness of different specimens. The comparison was conducted based on the average value for each group of specimens. As indicated by the data shown in Figure 11 and Table 5, the shear stiffness and capacity of the shear specimens exhibited the following patterns.

(1) In the load-increasing stage, the slope of the load–slip curve declined gradually, and the shear stiffness of the specimen gradually reduced.

(2) The assembled specimen exhibited much higher stiffness than the CIP specimen, while the assembled specimen had a slightly lower load capacity than the CIP specimen. The shear capacity and stiffness of the assembled shear connectors were 0.84 times and 2.46 times those of the CIP connectors, respectively. The high-strength grout locally reinforced the steel–concrete interface, resulting in reduced initial deformation and consequently higher stiffness of the prefabricated specimens. However, the initial failure

occurred in the conventional concrete regions, as the prefabrication approach compromised the concrete's structural integrity, ultimately leading to lower ultimate strength in the prefabricated specimens.

(3) For the assembled specimens featuring a perforated steel plate, the load capacity of the specimen with a 4-milimeter-thick steel plate was similar to that of the specimen with a 2-milimeter-thick steel plate. The stiffness of the 4 mm steel plate connectors increased by 42% compared to the 2 mm steel plate connectors.

Table 5. Bamboo scrimber–lightweight concrete shear connections' push-out test results [11].

Specimen ID	Ultimate Load	Load Capacity of a Single Shear Connector	Ultimate Slip	Stiffness
	P_{max} (kN)	1/2 P_{max} (kN)	Δ_{max} (mm)	K (kN/mm)
BPC04P	129.74	64.87	0.74	182.92
BPC04A	108.87	54.44	1.29	449.63
BPC02A	109.91	54.95	2.33	316.44

4. Shear Capacity Analysis

4.1. Analysis of the Perforated Steel Plate Connector Shear Mechanism

Perforated steel plate connectors in steel–concrete composite structures are commonly termed perforated rib plates or PBL shear keys as an abbreviation of the German term "perfobond leiste", which is translated as perfobond strip. Perforated steel plates possess a higher load capacity and shear stiffness than stud connectors, and their mechanical performance indicators are less strongly influenced by fatigue loads, showing characteristics typical of rigid connectors [16]. Perforated steel plate shear connectors embedded in concrete have complex load paths, with multiple factors affecting their shear performance. Taking the size of the perforations as an example, both excessively large and small perforation areas will reduce the shear performance of the connectors. This can be attributed to the through-rebars undergoing flexural deformation, with an enhanced restraining effect on concrete (Figure 12). When the perforation area is too small, the presence of through-rebars will prevent coarse aggregates from entering the perforations of the steel plate. When the perforation area is too large, the proportion of area occupied by the through-rebars will decrease, reducing their ability to restrain the concrete. The shear performance of the connector declines under both scenarios [17].

Limited research has been conducted on the utilization of perforated steel plates as connectors in BCC components. As a result, there are few reports in the literature regarding the load capacity of perforated steel plate connectors in BCC components. To explore methods for obtaining the shear capacity of perforated steel plate shear connectors, this study mainly utilized research the results and methods involving the load capacity of perforated steel plate connectors in steel–concrete composite components. Existing studies [18–25] have demonstrated that the main factors influencing the load capacity of perforated steel plate connectors include the perforation diameter of the perforated steel plate, the perforations being open or closed, the concrete strength and the strength of its stirrups, the diameter and angle of the through-rebars in the perforations, and the steel plate thickness.

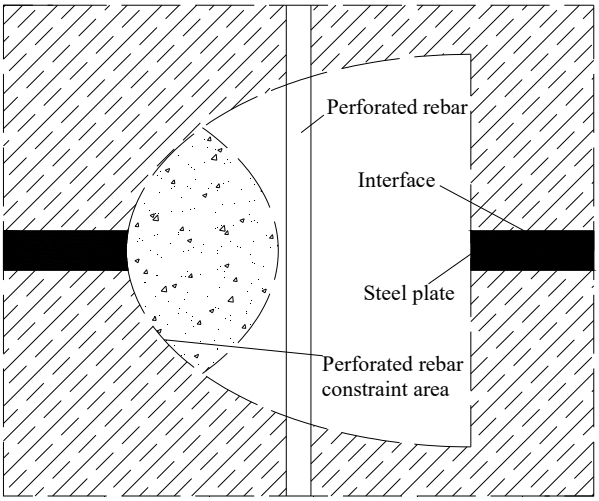

Figure 12. Confining region of the insert bar within the perforated steel plate connection.

In the present study, the BCC specimens were composed of assembled components. As a result, tight contact between the concrete and bamboo could not be achieved during the assembly process. When considering the shear capacity of the connectors, this work therefore ignored the friction at the interface between the concrete and bamboo. The shear capacity was derived based on four main components, as shown in Figure 13: (1) the concrete tenon columns in the perforations of the steel plate, (2) the through-rebars in the perforations of the steel plate, (3) the end bearing of the perforated steel plate, and (4) the reinforcing effect of the through-rebars.

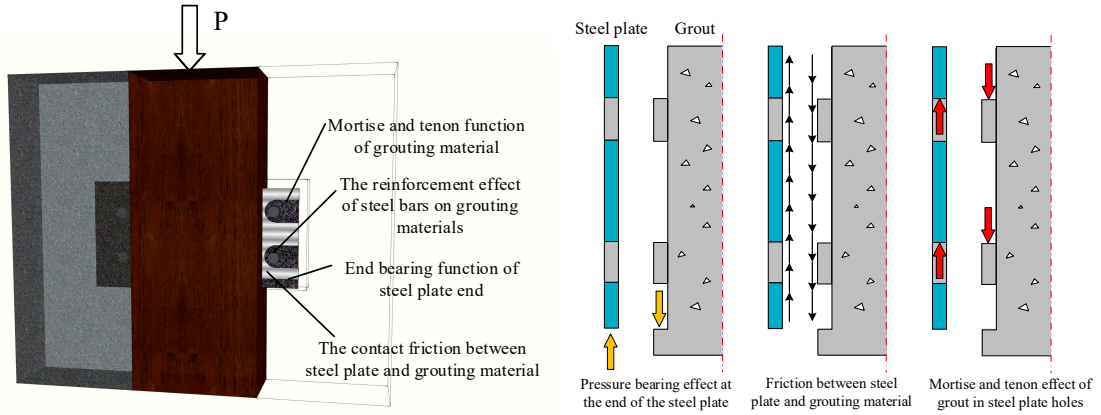

(**a**) force application points on the connector (**b**) shear capacity composition of the connector

Figure 13. Mechanical behavior of the perforated steel plate shear connector.

(1) Bearing force at the end of the steel plate

As illustrated in Figure 13, there was a positive correlation between the bearing force at the end of the steel plate and the product of the contact area between the end of the steel plate and the concrete and the average compressive stress in that area. The equation used to calculate the preliminary estimation is as follows:

$$P_{\mathrm{b}} = k_b \cdot t \cdot h \cdot f_{\mathrm{c}}, \tag{1}$$

where P_{b} represents the contribution of the end bearing of the steel plate to the shear capacity (N); k_{b} indicates the utilization coefficient of the concrete strength in the projected area of the end of the steel plate; t denotes the thickness of the perforated steel plate (mm); h

represents the embedment depth of the perforated steel plate in the concrete, i.e., the height of the connector (mm); and f_c indicates the compressive strength of the concrete (MPa).

(2) Contact friction between the steel plate and concrete

As depicted in Figure 14, the contact friction between the steel plate and the concrete comprised the shear capacity P_{Tr} along the shear failure surface contributed by the lateral restraining force T_r, which was comparable to the friction along the shear failure surface induced by the lateral restraint. A positive correlation was found between the contact friction between the steel plate and the concrete and the product of the contact area between the side of the steel plate and the concrete, in addition to the lateral bond strength in that area exerted by the concrete on the steel plate. This can be preliminarily obtained using the following equation:

$$P_{tr} = k_r \cdot \mu \cdot T_r = k_r \cdot \mu \cdot f_w \cdot h \cdot H, \quad (2)$$

where T_r, T_s, and T_c represent the total lateral restraining force, the lateral restraining force contributed by the through-rebars, and the lateral restraining force contributed by the concrete bond, respectively; P_{tr} indicates the contribution of the contact friction between the steel plate and the concrete (N); k_r denotes the utilization coefficient of the contact friction between the side of the steel plate and the concrete; μ refers to the friction coefficient between the steel plate and the concrete; f_w represents the lateral bond stress exerted by the concrete on the steel plate (MPa), which is linked to the concrete strength and is later substituted by the concrete strength; h indicates the depth of the perforated steel plate embedded in the concrete, i.e., the height of the connector (mm); and H denotes the length of the perforated steel plate, i.e., the dimension of the steel plate in the direction of the interface as well as that of the force (mm). P_{tr} could also be expressed as the product of the average bond strength at the interface, i.e., $\tau_0 = k_r \cdot \mu \cdot f_w$, and the interface contact area $h \cdot H$, namely, $P_r = 2 \cdot h \cdot H \cdot \tau_0$. According to reference [18], $\tau_0 = 0.054\, f_c + 0.1$.

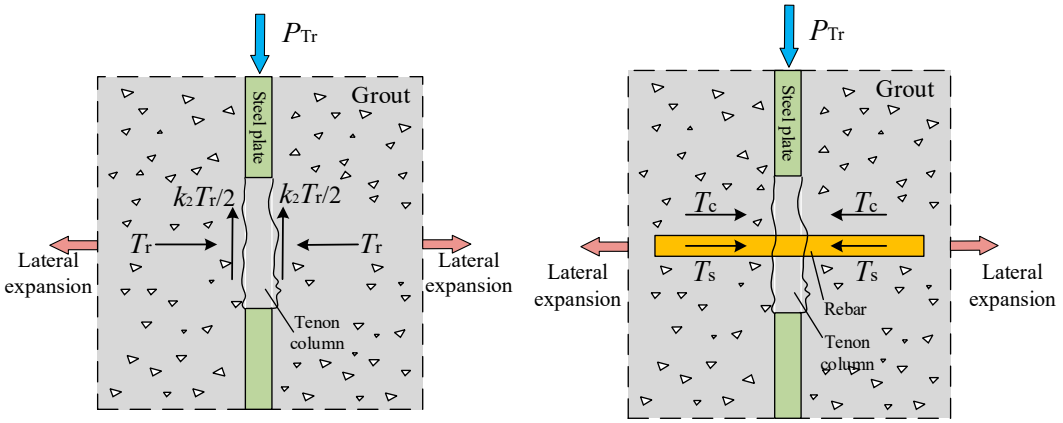

(**a**) contribution (**b**) composition of the lateral restraining force

Figure 14. Lateral restraint of the perforated steel plate shear connector.

(3) Force due to the mortise and tenon effect of concrete in steel plate perforations

As illustrated in Figure 15, the shear strength of the concrete tenon column controlled the degree to which this effect contributed to the load capacity. The force exhibited a positive correlation with the product of the concrete tenon column strength and the contact area between the steel plate perforation and the concrete tenon column. This can be preliminarily estimated using the following equation:

$$P_c = n \cdot k_c \cdot t \cdot d \cdot f_c, \quad (3)$$

where P_c represents the force contributed by the mortise and tenon effect of concrete in the steel plate perforations (N); n indicates the number of perforations in a single steel plate; k_c refers to the strength utilization coefficient of the concrete tenon column; t indicates the thickness of the perforated steel plate (mm); d represents the diameter of the perforation in the perforated steel plate (mm) (because the perforations in this experiment were not circular, d denotes the depth of the perforation, i.e., the dimension of the perforation in the direction perpendicular to the interface); and f_c represents the compressive strength of the concrete (MPa).

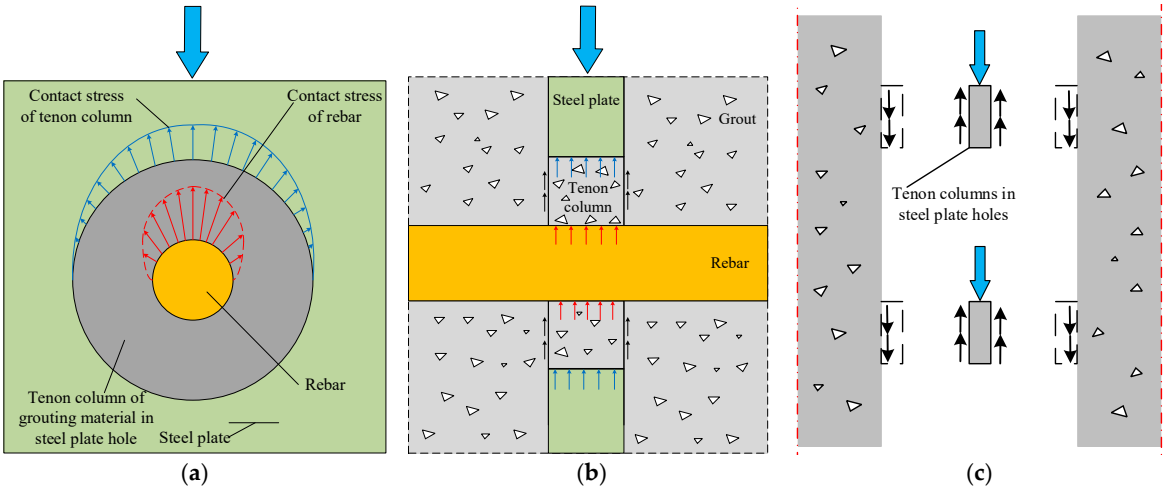

Figure 15. Shear stress distribution of the perforated steel plate shear connector. (**a**) Cross-section with the presence of a through-rebar. (**b**) Side view with the presence of a through-rebar. (**c**) Perforated steel plate with no through-rebar.

Previous reports containing similar conclusions [19] indicate that the shear capacity of a single perforation in the perforated steel plate shear connector, Q_{hole} (N), can be calculated as follows:

$$Q_{hole} = k_c \cdot \sqrt{t/d} \cdot d^2 \cdot f_c, \quad (4)$$

where k_c represents the strength utilization coefficient of the concrete tenon column, t indicates the thickness of the perforated steel plate (mm), d denotes the diameter of the perforations in the perforated steel plate (mm), and f_c refers to the compressive strength of the concrete (MPa). Furthermore, t/d was employed to characterize the variation in the effect of the perforation diameter on the load capacity with the thickness of the rib plate.

(4) Contribution of the reinforcing impact of through-rebars

As shown in Figure 15, the contribution of the added through-rebars to shear resistance was analyzed separately. The through-rebars were primarily responsible for the enhancement of the shear capacity of the concrete tenon column within the perforations. When through-rebars were not present, the shear capacity of the tenon column was primarily contributed by the bonded portions at either end of the tenon column. The tenon column was regarded as a beam with both ends fixed, and the bonded portion at each end served as a fixed support. The shear capacity of the tenon column was determined by the support reactions at either end, in addition to the strength of the tenon column itself, which was influenced by factors including the size of the tenon column and the concrete strength. When through-rebars were provided, it was equivalent to adding extra support to the tenon column at mid-span, which helped to improve the load capacity. However, the through-rebars occupied a portion of the volume of the tenon column, which

disadvantageously turned the tenon column into a hollow column. Therefore, further tests were needed to determine an appropriate balance for the diameter of the through-rebars.

Regarding the reinforcing effect of the through-rebars, the explanation provided by Zhu et al. [20] was considered clear and convincing. As illustrated in Figure 15, Zhu et al. [20] reported that when the specimen was subjected to load, the concrete tenon column within the perforation exhibited a tendency toward lateral expansion, and the through-rebars contributed lateral restraint against this expansion. According to the literature [18–25], the force contributed by the reinforcing effect of through-rebars was positively correlated with the product of their diameter and strength, which could be preliminarily estimated by:

$$P_y = \alpha \cdot n \cdot \frac{\pi \cdot d^2}{4} \cdot f_y, \quad (5)$$

where α denotes the utilization coefficient of the reinforcing effect of the through-rebars; n represents the number of perforations in the steel plate, which is also the number of through-rebars; d indicates the diameter of the through-rebars (mm); and f_y refers to the strength of the through-rebars (MPa).

Additionally, the perforated steel plate connectors used in this study differed from ordinary steel plates with circular perforations and could be referred to as perforated steel plate connectors with U-shaped notches. The design intention behind this type of steel plate configuration was to find a structural form suitable for the assembly construction of prefabricated components. This configuration allowed the embedded through-rebars in the prefabricated concrete to smoothly snap into the perforations of the perforated steel plate through the U-shaped notch during assembly. When conducting analytical research on shear capacity calculation methods, it was necessary to consider the similarities and differences between perforated steel plates with U-shaped notches and conventional perforated steel plates with circular perforations. While extensive research has been conducted on the latter, minimal research has been conducted on the former. According to the research results obtained by Zheng et al. [21], regardless of whether the perforated plate connectors had notches, steel–concrete connectors exhibited high load-bearing capacity in the direction perpendicular to the interface. Notches on the outer edges of circular perforations in the perforated plate connectors expanded the shear area, which increased the shear capacity and stiffness of the notched perforated steel plate by approximately 10% and 6%, respectively, while the peak slip was reduced by approximately 18%. Therefore, the shear capacities of steel plate connectors featuring circular and notched perforations did not differ significantly. Consequently, during the examination of the shear capacity of the perforated steel plate connectors with U-shaped notches, this study referred to the test results obtained for the steel plate connectors with circular perforations.

The above analysis clearly demonstrates that numerous factors affected the shear capacity of the perforated steel plate connectors, including (1) the strength of the concrete, (2) the diameter of the perforations in the steel plate, (3) the strength and diameter of the through-rebars, (4) the thickness of the perforated steel plate, (5) the spacing between perforations, (6) the stirrup ratio, and (7) additional random factors, such as whether the through-rebars were centered and whether coarse concrete aggregates infiltrated the gap between the steel plate and through-rebars. The shear capacity of perforated steel plate connectors was predominately determined by the following four factors: (1) the concrete tenon column within the perforations of the perforated steel plate, (2) the through-rebars within the perforations of the perforated steel plate, (3) the end bearing of the perforated steel plate, and (4) the reinforcing influence of the through-rebars. The contributions of these aspects of the shear capacity differed between loading stages, as well as the overall shear capacity. Therefore, the following subsection compares different analytical methods

to clarify the most appropriate technique for obtaining the shear capacity of the perforated steel plate connector.

4.2. Determination of the Shear Capacity of the Perforated Steel Plate Connector

For comparative analysis, this study obtained the equations used to calculate the shear capacity of the perforated steel plate connectors from several widely cited classical references, in addition to the latest research findings and relevant code standards. These existing formulas were employed to determine the shear capacity of the specimens in the present study to examine their applicability for BCC structures with perforated steel plates.

The findings of the present study indicated that the calculation formulas for the perforated steel plate shear connectors proposed in previous studies differed because they accounted for varying influencing factors. The major factors considered comprised the area and strength of the concrete tenon columns between perforations; the area and strength of the through-rebars; and the thickness, height, and strength of the perforated steel plates, as presented in Table 6.

Table 6. Formulas used to calculate the shear capacity of representative connections with perforated steel plate connectors.

No.	Reference	Calculation Formula	Factors Contributing to Shear Capacity Considered	Specific Parameters Involved	Steel Plate Type
1	Eurocode 4 [26]	$V_u = \frac{1.85[\pi(d^2-\phi_{st}^2)/4\cdot\sigma_{cd}+\pi\phi_{st}^2/4\cdot\sigma_{st}]-106.1\times10^3}{\gamma}$	Through-rebars, concrete tenon	①②③④	Single perforation
2	Leonhardt et al. [27]	$Q_u = 1.79d^2 f_c$	Concrete tenon	①③	Single perforation
3	Hosaka et al. [28]	$Q_u = 1.45\left[\left(d^2 - {d_s}^2\right)f_c + {d_s}^2 f_y\right] - 26100$	Through-rebars, concrete tenon	①②③④	Single perforation
4	Nishiumi et al. [29]	$Q_u = \begin{cases} 0.26A_c f_c + 1.23A_s f_y & A_s f_y / A_c f_c < 1.28 \\ 1.83A_c f_c & A_s f_y / A_c f_c \geq 1.28 \end{cases}$	Through-rebars, concrete tenon	①②③④	Single perforation
5	Oguejiofor et al. [30]	$q_u = 4.50htf_c' + 3.31nd^2\sqrt{f_c'} + 0.91A_{tr}f_{yr}$	Through-rebars, concrete tenon, end bearing of the steel plate	①②③④⑤⑥⑦	Multiple perforations
6	Zong et al. [31]	$V_u = \alpha_1\beta_1 A_c \cdot \sqrt{E_c f_c} + \alpha_2\beta_2 A_{tr} f_y$	Through-rebars, concrete tenon	①②③④⑧	Single perforation
7	JTG D64-2015 [32]	$Q_{su} = 1.4(d_p^2 - d_s^2)f_{cd} + 1.2d_s^2 f_{sd}$	Through-rebars, concrete tenon	①②③④	Single perforation
8	Hu et al. [33]	$Q_u = \alpha A_{tr} f_y + \beta A_{tr}' f_y' + \gamma A_c\sqrt{f_c}$	Through-rebars, concrete tenon, stirrups	①②③④⑨⑩	Single perforation
9	Xiao et al. [34]	$Q_u = \beta_1\xi(t/D)A_c f_c + \beta_2 A_{tr} f_y$	Through-rebars, concrete tenon	①②③④⑥⑨⑩	Single perforation
10	Al-Darzi et al. [35]	$V_u = 255.31 + 7.62\times10^{-4}\,htf_c' - 7.59\times10^{-7}A_r f_y + 2.53\times10^{-3}A_{sc}\sqrt{f_c'}$	Through-rebars, concrete tenon, end bearing of the steel plate	①②③④⑤⑥	Single perforation
11	Yang et al. [36]	$P_u = 5.15A_e f_{cu} + 5.14A_c f_{cu}^{0.57} + 2.24A_r f_y$	Through-rebars, concrete tenon, end bearing of the steel plate	①②③④⑤⑥	Single perforation
12	Hosain et al. [37]	$q = 0.590A_{cc}\sqrt{f_c'} + 1.233A_{tr}f_y + 2.871nd^2\sqrt{f_c'}$	Through-rebars, concrete tenon, side friction of the steel plate	①②③④⑤⑥⑦	Multiple perforations

Note: ① diameter of perforation, ② diameter of through-rebars, ③ concrete strength, ④ strength of through-rebars, ⑤ steel plate height, ⑥ steel plate thickness, ⑦ number of perforations in the steel plate, ⑧ elastic modulus of concrete, ⑨ stirrup strength, and ⑩ stirrup ratio.

Table 7 displays the shear capacities obtained for the specimens, in addition to their calculated shear capacities according to the aforementioned formulas. As shown in Figure 16, the formulas employed to calculate the shear capacity of perforated steel plate shear connectors were evaluated.

Table 7. Shear capacities of bamboo–concrete connections with perforated steel plate connectors (kN).

Specimen ID	Measured Value	Eurocode 4 [26]	Leonhardt et al. [27]	Hosaka et al. [28]	Nishiumi et al. [29]	Oguejiofor et al. [30]	Zong et al. [31]	JTG D64-2015 [32]	Hu et al. [33]	Xiao et al. [34]	Al-Darzi et al. [35]	Yang et al. [36]	Hosain et al. [37]
BPC02A	55.23	89.69	125.21	249.22	100.49	161.14	272.02	260.22	268.28	104.51	277.20	307.45	192.60
Measured value/calculate value	-	0.61	0.44	0.22	0.55	0.34	0.20	0.21	0.20	0.53	0.20	0.18	0.29
BPC04A	55.05	89.69	125.21	249.22	100.49	181.28	272.02	260.22	268.28	118.17	280.61	330.51	192.60
Measured value/calculate value	-	0.61	0.43	0.22	0.54	0.30	0.20	0.21	0.20	0.46	0.19	0.16	0.28
BPC04P	65.15	61.07	79.36	220.64	63.69	160.22	225.31	232.63	266.79	113.21	274.33	319.82	183.74
Measured value/calculate value	-	1.06	0.82	0.29	1.02	0.40	0.29	0.28	0.24	0.57	0.24	0.20	0.35

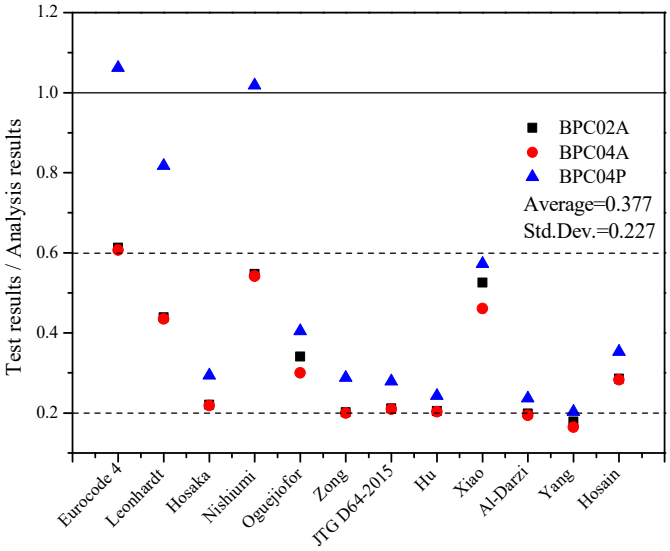

Figure 16. Assessment of equations used to calculate shear connections with perforated steel plate connectors.

As indicated by the data shown in Figure 16 and Table 7, the measured shear capacities of only a small number of specimens were close to the results obtained using the formulas. This indicates that the existing formulas could not be employed to directly calculate the shear capacity of the assembled bamboo–concrete shear connectors. The following conclusions were obtained based on comparisons.

(1) Utilizing the formulas for perforated section steel plate–concrete connectors generally yielded higher shear capacities for the bamboo–concrete connectors than the experimental measurements. Therefore, it is not appropriate to directly use the shear capacity calculation formulas for steel-concrete connectors to describe the shear capacity of bamboo–concrete connectors, as these equations are poorly applicable for the latter.

(2) Some equations provided more accurate calculations for CIP connectors (BPC04P group), with data points closer to the horizontal line with a ratio of measured to calculated values equal to 1, suggesting that some of the existing shear capacity calculation equations are more suitable for the CIP specimens. Because this study mainly focused on assembled specimens, it was necessary to conduct relevant analysis and modifications based on the construction method (assembled or CIP).

(3) The distribution of data points indicate that the ratio of measured to calculated values generally ranged from 0.2 to 0.6, suggesting that the measured and calculated values are significantly different.

The main reasons for deviations in calculations could be attributed to the effects of the following factors. (1) In this study, the steel plate had two perforations, while the equations in the referenced literature mostly addressed cases where the steel plate had a single perforation. In this study, the calculated value for the case of two perforations was obtained by doubling the value calculated using the formulas for a single perforation scenario, which possibly resulted in an overestimation. This was because the second perforation in a two-perforation plate bore less load than the first perforation. The first perforation was closer to the load and consequently underwent greater deformation, strain, and stress, thus carrying a greater portion of the load. (2) The steel plate in this study was relatively thin compared with the steel plates employed in the referenced literature, which enhanced the likelihood of stress concentrations inducing localized concrete failure, which in turn decreased the overall load capacity. (3) In previous works, perforated steel plate connectors were commonly welded to steel beams, while in the present study, the

connection between the perforated steel plate and bamboo beam was realized through slotting, embedding, and structural adhesive bonding, which ultimately produced a bonding strength that was weaker compared to welding. In the previous literature, concrete failure was defined as the type of failure corresponding to the peak load of steel–concrete connectors, while the failure mechanism examined in the bamboo–concrete connections in the present study likely proceeded in two stages. The first stage marked the failure of the structural adhesive, while concrete failure occurred during the second stage. It was possible that failure corresponding to the peak load in the bamboo–concrete connection was not concrete failure, but rather the failure of the structural adhesive. Consequently, although the ultimate failure in both cases was concrete failure, the factors influencing the peak load differed. (4) For the CIP specimens, the perforated steel plates used in this study had small perforation diameters and embedded through-rebars, making it difficult for coarse aggregates to enter the perforations, which was not conducive to the development of concrete strength. (5) For the assembled specimens, the difference in strength between the grout and prefabricated lightweight concrete blocks possibly had an adverse effect. (6) The shear capacity calculation formulas obtained by most researchers were based on their own experimental results. The variations in the materials, fabrication methods, and cumulative manufacturing errors employed for connectors by different researchers led to the discrepancy between the results calculated using the above analytical methods and the experimental results for the specimens in the current study.

The examination of different factors suggests that the shear capacity of the bamboo–concrete connector with perforated steel plates primarily consists of four aspects: the end bearing force of the steel plate, contact friction, and forces due to the influence of tenon columns and the reinforcing impact of through-rebars. The equation can be expressed in the following form:

$$P = \mathrm{a} \cdot t \cdot h \cdot f_{\mathrm{c}} + \mathrm{b} \cdot h \cdot H \cdot f_{\mathrm{c}} + \mathrm{c} \cdot n \cdot \frac{\pi \cdot D^2}{4} \cdot f_{\mathrm{c}} + \mathrm{d} \cdot n \cdot \frac{\pi \cdot d^2}{4} \cdot f_{\mathrm{y}}, \quad (6)$$

where a represents the utilization coefficient of the load-bearing capacity at the end of the steel plate; b indicates the utilization coefficient of the contact friction between the steel plate and concrete; c refers to the utilization coefficient of the mortise and the tenon effect of concrete inside the steel plate perforations; d denotes the utilization coefficient of the reinforcing influence of the through-rebars; t indicates the thickness of the perforated steel plate (mm); h refers to the depth of the perforated steel plate embedded inside the concrete, which is the same as height of the connector (mm); f_{c} represents the compressive strength of the concrete cylinder (MPa); n denotes the number of perforations in the steel plate, which is also the number of through-rebars; H indicates the length of the perforated steel plate, i.e., the size of the steel plate in the direction of the interface as well as in the direction of the force (mm); D denotes the diameter of the perforations in the steel plate (mm); d represents the diameter of the through-rebars (mm); and f_{y} refers to the strength of the through-rebars (MPa).

Chen et al. [16] reported that the end bearing of the steel plate, the friction between the side of the steel plate and the concrete, and the influence of the concrete tenon column contributed to the shear capacity at a ratio of 97:174:118, which is approximately equal to 1:1.7:1.2. Based on comparative analysis of the calculated values of the first three contributions, a reasonable and widely applicable formula could be derived in the form of the sum of the products of each term and a fixed numerical coefficient:

$$P = 22.5 \cdot \beta \cdot t \cdot h \cdot f_{\mathrm{c}} + \beta \cdot h \cdot H \cdot f_{\mathrm{c}} + 2.88 \cdot \beta \cdot n \cdot \frac{\pi \cdot D^2}{4} \cdot f_{\mathrm{c}} + \alpha \cdot n \cdot \frac{\pi \cdot d^2}{4} \cdot f_{\mathrm{y}}. \quad (7)$$

Yang et al. [36] demonstrated that the ratio of the capacity provided by the end bearing of the steel plate to the capacity contributed by the reinforcing effect of the through-rebars was 56% to 25%. Based on this ratio, as well as the ratio of the sum of the first three contributions to the fourth contribution, the relationship between α and β could be determined. By substituting β for α, the above formula could be transformed into the following form:

$$P = 22.5 \cdot \beta \cdot t \cdot h \cdot f_c + \beta \cdot h \cdot H \cdot f_c + 2.88 \cdot \beta \cdot n \cdot \frac{\pi \cdot D^2}{4} \cdot f_c + 0.53 \cdot \beta \cdot n \cdot \frac{\pi \cdot d^2}{4} \cdot f_y. \quad (8)$$

After rearranging terms, the following equation was obtained:

$$P = \beta \cdot (22.5 \cdot t \cdot h \cdot f_c + h \cdot H \cdot f_c + 2.88 \cdot n \cdot \frac{\pi \cdot D^2}{4} \cdot f_c + 0.53 \cdot n \cdot \frac{\pi \cdot d^2}{4} \cdot f_y). \quad (9)$$

Employing the experimental data and mathematical calculations, the average value of β was demonstrated to be 0.1113. Therefore, the final form of the equation obtained in this study was

$$P = 2.51 \cdot t \cdot h \cdot f_c + 0.11 \cdot h \cdot H \cdot f_c + 0.32 \cdot n \cdot \frac{\pi \cdot D^2}{4} \cdot f_c + 0.06 \cdot n \cdot \frac{\pi \cdot d^2}{4} \cdot f_y \quad (10)$$

The shear capacities calculated using the proposed formula were compared with the experimentally measured shear capacities, as depicted in Figure 17 and Table 8. This formula could be used to accurately predict the shear capacity of the specimens tested in the present work. However, a limited number of specimens were employed in this study, and further research based on a greater number of specimens is necessary. Currently, few reports have used perforated steel plates as connectors in BCC structures, making it difficult to validate the applicability of the proposed formula with data from other studies.

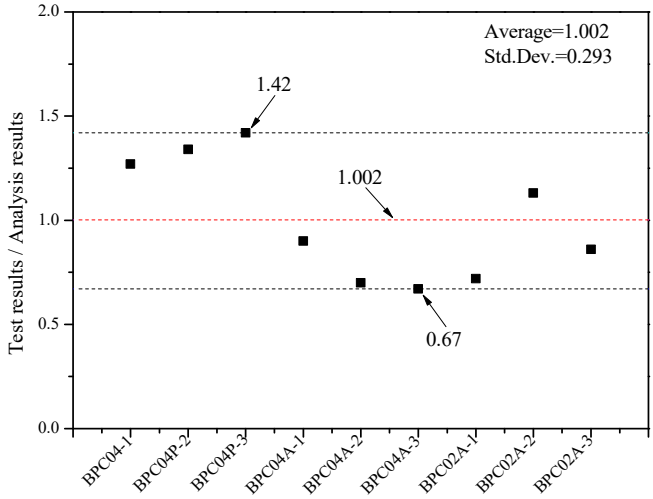

Figure 17. Assessment of the shear capacity of connections with perforated steel plate connectors.

To further validate the applicability of the proposed equation, we conducted a comprehensive analysis by collecting experimental capacity data of bamboo–concrete connections with perforated steel plates from the existing literature [3,10]. The collected data were systematically evaluated using our proposed equation, with the calculated capacities presented in Table 9. The comparative analysis, illustrated in Figure 18, demonstrates the correlation between the calculated capacities and experimental values from the literature. Statistical evaluation reveals that the ratio of measured to calculated values yielded a mean of 0.977 with a standard deviation of 0.221, indicating that the proposed equation provides

relatively accurate predictions for the shear capacity of bamboo–concrete connections with perforated steel plates.

Table 8. Experimental and analytical shear capacities of different perforated steel plate connectors.

Specimen ID	Measured Value (MPa)	Calculated Value (MPa)	Measured Value/Calculate Value
BPC04P-1	61.44	48.24	1.27
BPC04P-2	64.75	48.24	1.34
BPC04P-3	68.42	48.24	1.42
BPC04A-1	64.76	71.92	0.90
BPC04A-2	50.21	71.92	0.70
BPC04A-3	48.34	71.92	0.67
BPC02A-1	43.92	60.69	0.72
BPC02A-2	68.58	60.69	1.13
BPC02A-3	52.36	60.69	0.86
AVE	/	/	1.002
SD	/	/	0.293
COV	/	/	0.292

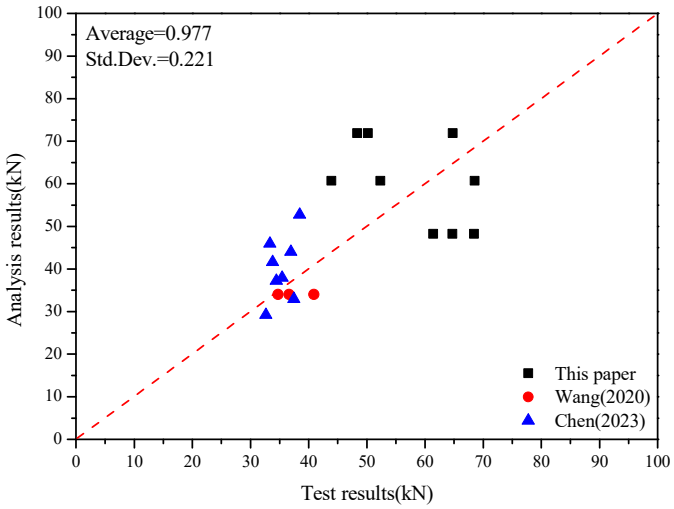

Figure 18. Evaluation of shear capacity equation for bamboo–concrete connections with perforated steel plate connectors [3,10].

Table 9. Evaluation of the shear capacity equation for bamboo–concrete connections with perforated steel plates.

Reference	Specimen ID	t (mm)	h (mm)	f_c (MPa)	H (mm)	n	D (mm)	D (mm)	f_y (MPa)	Measured Value (MPa)	Calculated Value (MPa)	Measured Value/Calculate Value
This work	BPC04P-1	4	40	35.47	100	2	25	12	534.88	61.44	48.24	1.27
	BPC04P-2	4	40	35.47	100	2	25	12	534.88	64.75	48.24	1.34
	BPC04P-3	4	40	35.47	100	2	25	12	534.88	68.42	48.24	1.42
	BPC04A-1	4	40	55.96	100	2	25	12	534.88	64.76	71.92	0.90
	BPC04A-2	4	40	55.96	100	2	25	12	534.88	50.21	71.92	0.70
	BPC04A-3	4	40	55.96	100	2	25	12	534.88	48.34	71.92	0.67
	BPC02A-1	2	40	55.96	100	2	25	12	534.88	43.92	60.69	0.72
	BPC02A-2	2	40	55.96	100	2	25	12	534.88	68.58	60.69	1.13
	BPC02A-3	2	40	55.96	100	2	25	12	534.88	52.36	60.69	0.86

Table 9. *Cont.*

Reference	Specimen ID	t (mm)	h (mm)	f_c (MPa)	H (mm)	n	D (mm)	D (mm)	f_y (MPa)	Measured Value (MPa)	Calculated Value (MPa)	Measured Value/Calculate Value
Wang [3]	P1	2	40	35.6	100	2	25	0	0	36.63	33.99	1.08
	P2	2	40	35.6	100	2	25	0	0	40.91	33.99	1.20
	P3	2	40	35.6	100	2	25	0	0	34.75	33.99	1.02
Chen [10]	B502000	2	40	34.7	100	2	20	0	0	32.66	29.21	1.12
	B502008	2	40	34.7	100	2	20	8	618.13	37.48	32.94	1.14
	B502012	2	40	34.7	100	2	20	12	593.05	34.46	37.25	0.93
	B502016	2	40	34.7	100	2	20	16	615.45	36.96	44.05	0.84
	B503000	2	40	34.7	100	2	30	0	0	35.44	37.93	0.93
	B503008	2	40	34.7	100	2	30	8	618.13	33.81	41.65	0.81
	B503012	2	40	34.7	100	2	30	12	593.05	33.34	45.97	0.73
	B503016	2	40	34.7	100	2	30	16	615.45	38.46	52.77	0.73

Note: t indicates the thickness of the perforated steel plate (mm); h refers to the depth of the perforated steel plate embedded inside the concrete, which is the same as height of the connector (mm); f_c represents the compressive strength of the concrete cylinder (MPa); n denotes the number of perforations in the steel plate, which is also the number of through-rebars; H indicates the length of the perforated steel plate, i.e., the size of the steel plate in the direction of the interface as well as in the direction of the force (mm); D denotes the diameter of the perforations in the steel plate (mm); d represents the diameter of the through-rebars (mm); and f_y refers to the strength of the through-rebars (MPa).

5. Conclusions

This study performed experimental analysis to investigate the shear performance of assembled bamboo scrimber–lightweight concrete shear connectors. Three groups of nine bamboo scrimber–lightweight concrete shear connectors featuring different parameters were designed and fabricated for use in push-out tests conducted during the experiments. The shear capacity of the connector was analyzed, and the following major conclusions were drawn:

(1) The damage of shear connector was primarily related to the deformation of the perforated steel plate, in addition to small areas featuring concrete spalling, which led to extensive slippage between the bamboo and concrete that ultimately resulted in connection failure. The bamboo material did not exhibit significant damage, with an insignificant difference in the failure modes between the CIP and assembled specimens.

(2) The load–slip curve of the shear connector was characterized by three rough stages. During the first stage, the connector was effectively connected to the bamboo and concrete, which ensured reliable shear transfer, and the load and relative slip of the specimen exhibited an approximately linear relationship. The load increase rate significantly declined during the second stage, while the slip rapidly increased, yielding a nonlinear load–slip curve, which was mainly caused by reduced shear stiffness induced by the local cracking of the concrete. The curve began to decrease during the third stage, which was primarily caused by local cracking and spalling in the concrete block, the yielding deformation of the connectors, and decreased bonding strength between the connector and concrete.

(3) The shear capacity and stiffness of assembled BCC shear connectors were 0.84 times and 2.46 times those of CIP connectors, respectively. The stiffness of the 4 mm steel plate connectors increased by 42% compared to the 2 mm steel plate connectors. The influence of the thickness of the perforated steel plate had a negligible impact on the shear capacity of the shear connector.

(4) This study calculated the slip distribution of the shear connector utilizing the full-field displacement data measured using DIC. During the early loading stage, the connector transferred the load stably. In the process of loading, the shear stiffness of the specimen continuously declined. Before the ultimate load was reached, the slip values on the left and right sides of the specimen were found to be approximately the same, which reflected the occurrence of uniform loading on the connectors on either side without eccentric loading.

(5) Analysis showed that the shear capacity of the BBC primarily consisted of four aspects: the end bearing force of the steel plate, contact friction, and forces due to the

influence of tenon columns and the reinforcing impact of through-rebars. A formula for obtaining the shear capacity of perforated steel plate connectors in the BCC structure has been proposed, and the standard deviation of the ratio between analytical and test values was 0.293.

Author Contributions: Z.W. contributed to examination of all of the tests and analysis of the data and was a major contributor in writing the manuscript. L.C. contributed to the design of this analysis study and discussion of the obtained results. H.L. contributed to examination of all of the tests. All authors have read and agreed to the published version of the manuscript.

Funding: This research was funded by the Natural Science Foundation (2022AH050590) of the Educational Committee of Anhui Province, China; the Natural Science Foundation (2021ZR10zd) of Bengbu University, China; the Project of Industry and School and Research Institution (LS0232) of Bengbu University, China; the Ministry of Education's Industry School Cooperation Collaborative Education Project (220605848083139); and the Bengbu Science and Technology Plan Project (2023hm04), China.

Data Availability Statement: The original contributions presented in this study are included in the article. Further inquiries can be directed to the corresponding author.

Conflicts of Interest: The authors declare no conflicts of interest.

References

1. Li, W.; Long, Y.; Huang, J.; Lin, Y. Axial load behavior of structural bamboo filled with concrete and cement mortar. *Constr. Build. Mater.* **2017**, *148*, 273–287. [CrossRef]
2. Wang, Z.; Wei, Y.; Hu, Y.; Chen, S.; Zhao, K. An investigation of the flexural performance of bamboo-concrete composite beams with precast light concrete slabs and dowel connectors—ScienceDirect. *J. Build. Eng.* **2021**, *41*, 102759. [CrossRef]
3. Wang, Z.; Wei, Y.; Li, N.; Zhao, K.; Ding, M. Flexural behavior of bamboo–concrete composite beams with perforated steel plate connections. *J. Wood Sci.* **2020**, *66*, 4. [CrossRef]
4. Shan, B.; Wang, Z.Y.; Li, T.Y.; Xiao, Y. Experimental and Analytical Investigations on Short-Term Behavior of Glubam-Concrete Composite Beams. *J. Struct. Eng.* **2020**, *146*, 04019217. [CrossRef]
5. Li, T.; Chen, J.Q.; Xiao, Y. Structural behavior of fully prefabricated glubam-concrete composite beams constructed of innovative connectors. *Eng. Struct.* **2024**, *308*, 117985. [CrossRef]
6. Wang, Z.; Wang, F.; Liu, H. Digital image correlation-based investigation of the shear performance of connection systems of assembled bamboo scrimber–lightweight concrete composite beams. *Materials* **2024**, *17*, 3268. [CrossRef]
7. Shan, B.; Li, T.; Deng, J. Experimental research on novel RPC-steel composite connections for prefabricated glubam-concrete composite beams. *Constr. Build. Mater.* **2022**, *23*, 127397. [CrossRef]
8. Shan, B.; Xiao, Y.; Zhang, W.; Liu, B. Mechanical behavior of connections for glubam-concrete composite beams. *Constr. Build. Mater.* **2017**, *143*, 158–168. [CrossRef]
9. Wang, Z.; Yang, W. Comparative study on mechanical behavior bamboo-concrete connections and wood-concrete connections. *Front. Mater.* **2020**, *7*, 587580. [CrossRef]
10. Chen, S.; Wei, Y.; Wang, G.; Zhao, K.; Yang, B. Experimental investigation on shear behavior of bamboo-concrete composite structure with perforated steel plate connection. *J. Build. Eng.* **2023**, *79*, 107795. [CrossRef]
11. Wei, Y.; Wang, Z.; Chen, S.; Zhao, K.; Zheng, K. Structural behavior of prefabricated bamboo-lightweight concrete composite beams with perforated steel plate connectors. *Arch. Civ. Mech. Eng.* **2021**, *21*, 15. [CrossRef]
12. *D143-09*; Standard Test Method for Small Clear Specimens of Timber. ASTM: Philadelphia, PA, USA, 1994.
13. *GB/T 50081-2019*; Standard for Test Methods of Concrete Physical and Mechanical Properties. Architecture & Building Press: Beijing, China, 2019.
14. *GB/T 228.1-2010*; Metallic Materials-Tensile Testing-Part 1: Method of Test at Room Temperature. Standards Press of China: Beijing, China, 2010.
15. *GB/T 50448-2015*; Technical Code for Application of Cementitious Grout. China Architecture & Building Press: Beijing, China, 2015.
16. Chen, H.; Guo, Z.; Liu, Y. Experimental study on shear capacity of inclined PBL shear connector. *J. Build. Struct.* **2020**, *41*, 209–218. [CrossRef]
17. Zhao, C.; Liu, Y.; Zheng, S. Experimental analysis of shear behavior of oval perfobond connector. In Proceedings of the 3rd International Conference on Transportation Engineering, Chengdu, China, 23–25 July 2011; ASCE: Reston, VA, USA, 2011; pp. 1983–1988. [CrossRef]

18. Zhen, S.; Deng, G.; Yang, Y. Experimental study of bond-slip performance between steel and concrete in steel reinforced concrete structures. *Eng. Mech.* **2003**, *20*, 63–69.
19. Hosaka, T.; Mitsukik, K.; Hiragih, H. An experimental study on shear characteristics of perfobond strip and its rational strength equations. *J. Struct. Eng.* **2000**, *46*, 1593–1604.
20. Zhu, W.; Cui, Y.; Liu, Y. Research on shear strength of perfobond rib connectors. *J. Build. Struct.* **2017**, *38*, 129–136. [CrossRef]
21. Zheng, S.; Liu, Y. Experimental investigation on shear and uplift behavior of notched perfobond connector. *China J. Highw. Trans.* **2013**, *26*, 119–124.
22. Zheng, S.; Liu, Y.; Yoda, T. Parametric study on shear capacity of circular-hole and long-hole perfobond shear connector. *J. Constr. Steel Res.* **2016**, *117*, 64–80. [CrossRef]
23. Kim, S.; Kim, K.; Park, S. Comparison of hysteretic performance of stubby Y-type perfobond rib and stud shear connectors. *Eng. Struct.* **2017**, *147*, 114–124. [CrossRef]
24. Gu, J.; Liu, D.; Deng, W. Experimental study on the shear resistance of a comb-type perfobond rib shear connector. *J. Constr. Steel Res.* **2019**, *158*, 279–289. [CrossRef]
25. Li, X.; Hu, Z.; Fan, L. Experimental investigation of perfobond hoop shear connector's bearing capacity and slip. *Eng. Struct.* **2019**, *198*, 109461. [CrossRef]
26. *EN 1994-1-1*; Eurocode 4: Design of Composite Steel and Concrete Structures—Part 1.1: General Rules and Rules for Buildings. European Committee for Standardization (CEN): Brusseles, Belguim, 2004.
27. Leonhardt, F.; Andra, W.; Andra, H. Neues, vorteilhaftes verbundmittel für stahlverbund-tragwerke mit hoher dauerfestigkeit. *Beton-und Stahlbetonbau* **1987**, *82*, 325–331. [CrossRef]
28. Hosaka, T. Study on shear strength and design method of perfobond strip. *J. Struct. Eng.* **2002**, *48*, 1265–1272.
29. Nishiumi, K.; Okimoto, M. Shear strength of perfobond rib shear connector under the confinement. *Doboku Gakkai Ronbunshu* **2010**, *633*, 193–203. [CrossRef] [PubMed]
30. Oguejiofor, E.; Hosain, M. Numerical analysis of push-out specimens with perfobond rib connectors. *Comput. Struct.* **1997**, *62*, 617–624. [CrossRef]
31. Zong, Z.; Che, H. Study on static load and fatigue test of shear connectors. *J. Fuzhou Univ.* **1999**, *27*, 61–66.
32. *JTG D64-2015*; Specifications for Design of Highway Steel Bridge. Communications Press: Beijing, China, 2015.
33. Hu, J.; Hou, W.; Ye, M. Study of influence factors and formula for the bearing capacity of PBL shear connectors. *J. Railw. Sci. Eng.* **2007**, *4*, 12–18. [CrossRef]
34. Xiao, L.; Qiang, S.; Li, X. Research on mechanical performance of PBL shear connectors considering the thickness of perforated plate. *Eng. Mech.* **2012**, *29*, 282–288. [CrossRef]
35. AL-Darzi, S.; Chen, A.; Liu, Y. Finite element simulation and parametric studies of perfobond rib connector. *Am. J. Appl. Sci.* **2007**, *4*, 122–127. [CrossRef]
36. Yang, Y.; Chen, Y. Experimental study on the shear capacity of PBL shear connectors. *Eng. Mech.* **2018**, *35*, 89–96. [CrossRef]
37. Oguejiofor, E.; Hosain, M. A parametric study of perfobond rib shear connectors. *Can. J. Civ. Eng.* **1994**, *21*, 614–625. [CrossRef]

Disclaimer/Publisher's Note: The statements, opinions and data contained in all publications are solely those of the individual author(s) and contributor(s) and not of MDPI and/or the editor(s). MDPI and/or the editor(s) disclaim responsibility for any injury to people or property resulting from any ideas, methods, instructions or products referred to in the content.